catalysts

MDPI

Article

The Effect of Transition Metal Substitution in the Perovskite-Type Oxides on the Physicochemical Properties and the Catalytic Performance in Diesel Soot Oxidation

Liliya V. Yafarova [1,*], Grigory V. Mamontov [2], Irina V. Chislova [1], Oleg I. Silyukov [1] and Irina A. Zvereva [1,*]

[1] Institute of Chemistry, St. Petersburg State University, 199034 St. Petersburg, Russia; i.v.chislova@gmail.com (I.V.C.); oleg.silyukov@spbu.ru (O.I.S.)
[2] Chemical Faculty, Tomsk State University, 36, Lenin Ave., 634050 Tomsk, Russia; grigoriymamontov@mail.ru
* Correspondence: liliyayafarova@gmail.com (L.V.Y.); irina.zvereva@spbu.ru (I.A.Z.)

Abstract: The paper is focused on the Fe for Co substitution effect on the redox and catalytic properties in the perovskite structure of $GdFeO_3$. The solid oxides with the composition $GdFe_{1-x}Co_xO_3$ (x = 0; 0.2; 0.5; 0.8; 1) were obtained by the sol-gel method and characterized by various methods: X-ray diffraction (XRD), temperature-programmed reduction (H_2-TPR), N_2 sorption, temperature-programmed desorption of oxygen (TPD-O_2), simultaneous thermal analysis (STA), and X-ray photoelectron spectroscopy (XPS). The H_2-TPR results showed that an increase in the cobalt content in the $GdFe_{1-x}Co_xO_3$ (x = 0; 0.2; 0.5; 0.8; 1) leads to a decrease in the reduction temperature. Using the TPD-O_2 and STA methods, the lattice oxygen mobility is increasing in the course of the substitution of Fe for Co. Thus, the Fe substitution in the perovskite leads to an improvement in the oxygen reaction ability. Experiments on the soot oxidation reveal that catalytic oxidation ability increases in the series: $GdFe_{0.5}Co_{0.5}O_3$ < $GdFe_{0.2}Co_{0.8}O_3$ < $GdCoO_3$, which is in good correlation with the increasing oxygen mobility according to H2-TPR, TPD-O_2, and STA results. The soot oxidation over $GdFeO_3$ and $GdFe_{0.8}Co_{0.2}O_3$ is not in this range due to the impurities of iron oxides and higher specific surface area.

Keywords: perovskites; transition metal oxides; temperature-programmed reaction; soot oxidation

Citation: Yafarova, L.V.; Mamontov, G.V.; Chislova, I.V.; Silyukov, O.I.; Zvereva, I.A. The Effect of Transition Metal Substitution in the Perovskite-Type Oxides on the Physicochemical Properties and the Catalytic Performance in Diesel Soot Oxidation. *Catalysts* **2021**, *11*, 1256. https://doi.org/10.3390/catal11101256

Academic Editor: Gilles Berhault

Received: 30 September 2021
Accepted: 16 October 2021
Published: 19 October 2021

1. Introduction

Diesel vehicles are widely used around the world due to their low fuel consumption, low maintenance costs, and low carbon dioxide emissions. At the same time, soot particles are among the products of incomplete combustion of diesel fuel and a dangerous pollutant that can cause serious diseases and adversely affect the environment [1]. Catalytic oxidation is the main way to reduce soot emissions. Usually, diesel soot is oxidized at temperatures above 600 °C, and the use of the catalysts leads to a decrease in the oxidation temperature. To date, various materials have been studied as catalysts for soot oxidation [2], and the best results are observed for the systems based on noble metals [3], transition metal oxides [4], and perovskites [5].

Due to their high thermal stability, low cost, and diverse physical-chemical properties, the perovskite-type mixed oxides are considered the promising catalysts for NO_x reduction [6] and oxidation of CO [7], hydrocarbons [8,9], and soot [10]. The oxides of this type can be described by the general formula ABO_3, where A is a cation of rare earth, alkali, or alkaline earth metal, and cation B is usually a transition metal of the 3d, 4d, or 5d group [11]. The opportunity for partial replacement of cation A and/or B allows creating a wide variety of complex mixed oxides with the modified physical-chemical and redox properties. On the one hand, partial replacement of element A with ions having a lower valency produces structural defects, such as anionic and cationic vacancies, and a change in the oxidation state of metal B to maintain electroneutrality of the compound [12]. At the same time, due to the ability of

the transition metal to be in several oxidation states, the perovskites, depending on external conditions, can accumulate oxygen non-stoichiometry. As a result, such defective structures have oxygen mobility and can generate active oxygen on the surface.

In perovskites, two types of oxygen can be distinguished, namely, surface and lattice ones [13]. Numerous studies show that the lattice oxygen mobility is a key factor in the mechanism of oxidative reactions, e.g., when methane is oxidized on perovskites, the lattice is a source of active oxygen participating in the reaction, which migrates to the surface followed by its replenishing from the gas phase [11,14]. It was also established that surface oxygen is very active and contributes to its complete oxidation during the methane oxidation, while the bulk oxygen facilitates the methane partial oxidation [15]. However, to date, the effect of the transition metal in position B on the formation of various types of oxygen and their mobility in perovskites remains incompletely studied.

Our previous studies focused on the study of the effect of the nature and degree of substitution of the transition metal in perovskite-like oxides $GdB_xFe_{1-x}O_3$ (x = 0; 0.2; 0.5; 0.8; 1, B = Co; Mn) on the catalytic properties in the reaction of dry reforming of methane and the Fischer-Tropsh synthesis [16–18]. It was found that the substitution of Co for Fe in $GdFe_{1-x}Co_xO_3$ (x = 0; 0.2; 0.5; 0.8; 1) leads to an increase in catalytic activity and an increase in the cobalt content prevents the deactivation of catalysts due to surface carbonization. We supposed that the decrease in surface carbonization is due to various types of oxygen present in perovskites.

Thus, this work aims to study the effect of the complete and partial substitution of Fe atoms for Co on the physical-chemical and redox properties of the $GdFeO_3$ perovskite as well as to find the relation between the ability to participate in the soot combustion process and the presents of different types of oxygen.

2. Results

Figure 1 demonstrates the XRD results for the as-prepared samples. All the characteristic peaks in the patterns can be assigned to the orthorhombic perovskite-type structure $GdCoO_3$ (PDF-ICDD 00-025-1057), $GdFeO_3$ (PDF-ICDD 01-072-9908), and their solid solutions. The XRD results show that the partial B-site substitution of Fe by Co in the $GdFe_{1-x}Co_xO_3$ (x = 0; 0.2; 0.5; 0.8; 1) showed a slightly shift of diffraction peaks towards higher values of 2θ compared to $GdFeO_3$ and monotonic decrease of cell parameters (Table 1) a, b, c in row $GdFe_{1-x}Co_xO_3$ (x = 0; 0.2; 0.5; 0.8; 1). These results correlated with the reduced size of cobalt cations ($R(Co^{3+})$ = 0.610 Å) compared with iron ($R(Fe^{3+})$ = 0.645 Å) [19]. This fact substantiates the Fe substitution by Co into the sites of the $GdFeO_3$ crystal structure and the formation of solid solutions.

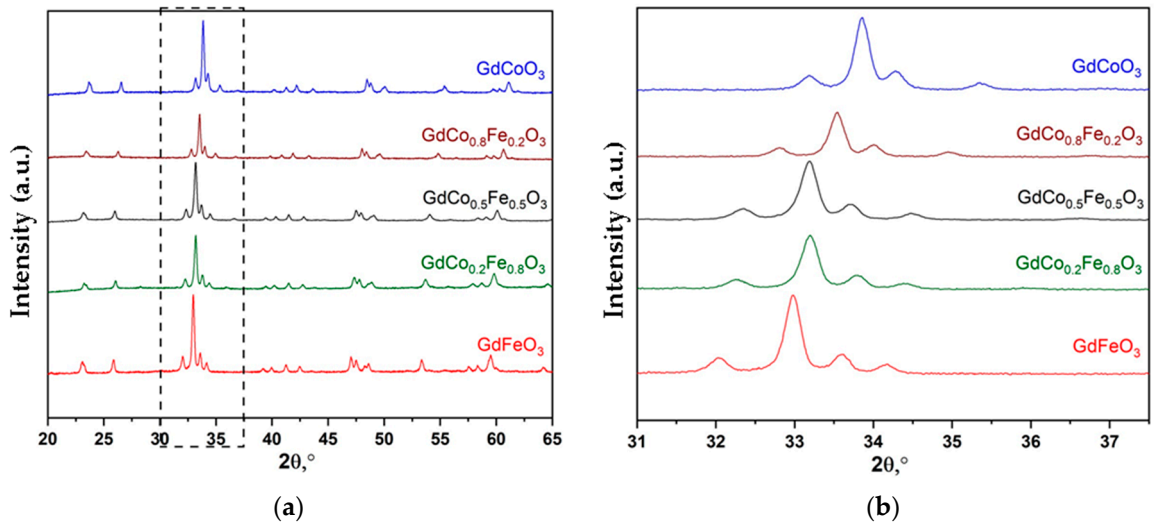

Figure 1. XRD patterns of as-prepared $GdFe_{1-x}Co_xO_3$ (x = 0; 0.2; 0.5; 0.8; 1) samples (**a**) full pattern; (**b**) zoom-in on the peak range.

Table 1. The properties of samples synthesized.

Sample	x	Lattice Parameters (Å)		Crystallite Size (nm)	S_{BET} (m^2/g)	Loading of Elements According to ICP (wt%)		
		Exper.	Liter.			Fe	Co	Fe/Co
$GdFeO_3$	0	a = 5.606 (8) b = 7.671 (0) c = 5.352 (1)	a = 5.616 b = 7.669 c = 5.349 [20]	53.4	10	22	-	-
$GdFe_{0.8}Co_{0.2}O_3$	0.2	a = 5.597 (9) b = 7.654 (7) c = 5.340 (9)	a = 5.550 b = 7.641 c = 5.345 [19]	47.3	3	15	4	3.75
$GdFe_{0.5}Co_{0.5}O_3$	0.5	a = 5.508 (5) b = 7.671 (2) c = 5.291 (5)	-	50.5	3	9.3	9.4	0.99
$GdFe_{0.2}Co_{0.8}O_3$	0.8	a = 5.439 (4) b = 7.498 (9) c = 5.253 (5)	a = 5.439 b = 7.498 c = 5.258 [19]	65.2	3	13	15	0.87
$GdCoO_3$	1	a = 5.394 (1) b = 7.566 (3) c = 5.225 (0)	a = 5.392 b = 7.471 c = 5.221 [21]	59.9	2	-	21	-

The bulk elements of these oxides are reflected by the ICP measurements, as displayed in Table 1. The experimentally obtained data are in good agreement with the theoretical content of the elements in the prepared $GdFe_{1-x}Co_xO_3$ compounds (x = 0; 0.2; 0.5; 1). However, for the $GdFe_{0.2}Co_{0.8}O_3$ sample (x = 0.8), the obtained results demonstrated a significant deviation of the iron content from the theoretical values that is most likely due to the presence of an impurity phase of iron oxide. The particle sizes of oxides were calculated based on XRD data using the Scherrer equation; Table 1 shows the calculated results. The samples' specific surface area (SBET) is ~3 m^2/g, and only the sample $GdFeO_3$ is characterized by S_{BET} of 10 m^2/g. Generally, the tendency of increasing the S_{BET} as the Fe amount increased was observed.

The surface composition and chemical state of the elements of the $GdFe_{1-x}Co_xO_3$ (x = 0; 0.2; 0.5; 0.8; 1) samples was investigated by XPS. The intensive lines of Gd3d, Fe2p, Co2p, O1s, and C1s were observed within the binding energy range of 0–1400 eV, and no lines corresponded to the other elements. The chemical states of Fe and Co metals and O in the investigated samples are detailed by fitting the XPS curves as shown in Figure 2.

The Co2p spectra (Figure 2a) also exhibit two major peaks with two satellite ones. The two major components, namely $Co2p_{3/2}$ and $Co2p_{1/2}$, are located at 779.80 eV and 795.1 eV for sample $GdCoO_3$ (x = 1), 779.19 eV and 794.09 eV for sample $GdFe_{0.2}Co_{0.8}O_3$ (x = 0.8), 779.90 eV and 794.82 eV for sample $GdFe_{0.5}Co_{0.5}O_3$ (x = 0.5), and 779.65 eV and 794.63 eV for sample $GdFe_{0.8}Co_{0.2}O_3$ (x = 0.2), respectively. The values of spin orbit splitting energy of $Co2p_{3/2}$ and $Co2p_{1/2}$ are ~15 eV. The existence of mixed oxides with Co^{2+} and Co^{3+} [19] was also confirmed by the two satellite peaks presented at the high binding energy sides [22]. It is noteworthy that the XPS peaks of $Co2p_{3/2}$ and $Co2p_{1/2}$ for all $GdFe_{1-x}Co_xO_3$ samples (x = 0.2; 0.5; 0.8; 1) are broad, indicating the existence of additional Co oxidation state. Table 2 lists the calculated ratios of the internal peak areas of the deconvoluted fitting curves of Co^{2+}/Co^{3+} for all investigated samples.

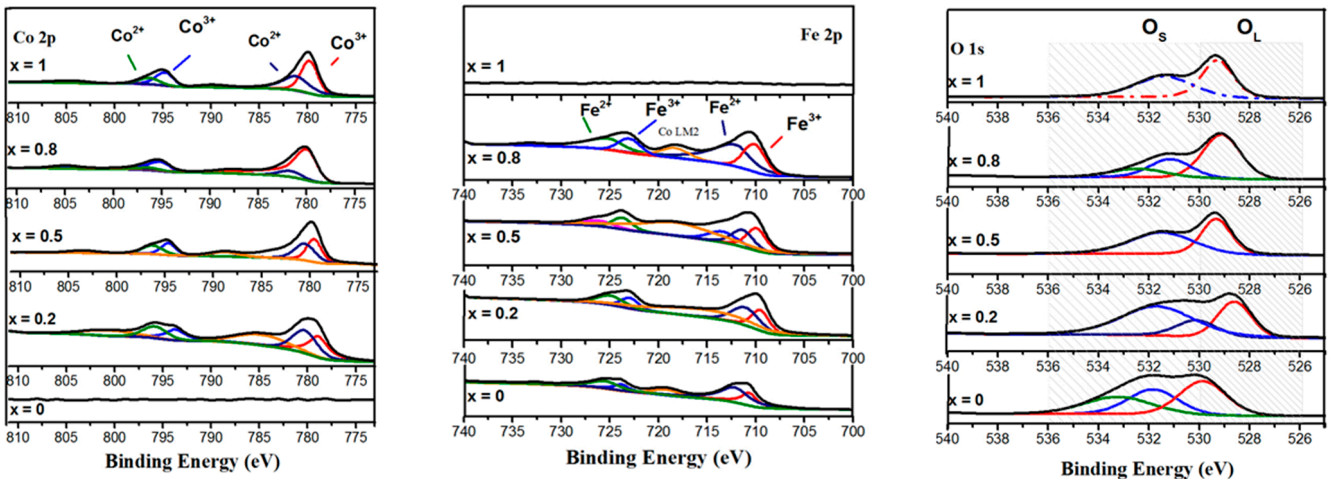

Figure 2. XPS spectra of (**a**) Co2p; (**b**) Fe2p and (**c**) O1s bands for $GdFe_{1-x}Co_xO_3$ (x = 0; 0.2; 0.5; 0.8; 1) samples.

Table 2. The surface compositions of $GdFe_{1-x}Co_xO_3$ (x = 0; 0.2; 0.5; 0.8; 1) samples obtained by XPS analysis.

Samples	Atomic Concentration (at. %)					Atomic Ratio		
	Gd	Co	Fe	O_s	O_l	$Co^{2+}/Co^{2+} + Co^{3+}$	$Fe^{2+}/Fe^{2+} + Fe^{3+}$	O_s/O_l
$GdFeO_3$	23.60	-	16.32	36.27	23.80	-	0.64	1.52
$GdFe_{0.8}Co_{0.2}O_3$	18.31	6.56	12.66	23.28	39.19	0.51	0.43	0.59
$GdFe_{0.5}Co_{0.5}O_3$	20.31	11.11	8.39	27.03	33.13	0.50	0.58	0.81
$GdFe_{0.2}Co_{0.8}O_3$	20.19	15.96	17.62	20.82	25.41	0.13	0.58	0.82
$GdCoO_3$	18.19	21.99	-	26.61	32.21	0.47	-	0.83

Figure 2b shows the XPS spectra of Fe characterized by two-peak spectra with low $Fe2p_{3/2}$ and high $Fe2p_{1/2}$ binding energies. The binding energy of the X-ray photoelectron peak of Fe depends on the chemical state and environment of the atoms. The positions of the $Fe2p_{3/2}$ peaks for all studied samples are in the range of 709.87–711.92 eV, while those of the $Fe2p_{1/2}$ peaks are 723.06–724.88 eV. The established values of the positions of the $Fe2p_{3/2}$ and $Fe2p_{1/2}$ peaks corresponded to the standard values of Fe^{2+} and Fe^{3+} [23], the presence of Fe in several states was also confirmed by the asymmetry of the Fe2p peaks [24]. For the $GdFe_{0.2}Co_{0.8}O_3$ compound (x = 0.8), the atomic concentration deviated from the theoretical value, which was consistent with the ICP results and confirmed the presence of an impurity phase of iron.

Figure 2c shows the fitted O1s peaks of adsorbed oxygen species, including chemisorbed oxygen, carbonate species, and adsorbed molecular water (denoted as O_s) at 530–534 eV as well as lattice oxygen species (denoted as O_l) at 528.57–529.67 eV [12,25]. The O_s concentration defined as O_s/O_l was calculated based on the area of the corresponding peaks and is given in Table 2. The O_s/O_l ratio in the compounds $GdFe_{1-x}Co_xO_3$ (x = 0.2; 0.5; 0.8; 1) increases with an increase in the amount of cobalt, these four samples have almost the same surface area values with respect to the $GdFeO_3$ (x = 0) compound, and higher S_{BET} value and higher O_s/O_l ratio are observed. These data demonstrate that the amount of O_s correlates well with surface area values. The Gd4d peaks for all studied samples corresponds to Gd^{3+} at 138.0 eV according to the reported [26].

Figure 3a shows the TPR profile for the obtained compounds and cobalt and iron oxides. Table 3 shows an estimate of the amount of H_2 consumed and the degree of reduction. For all the compounds studied, two successive reduction stages are observed: a low-temperature peak before 510 °C and a high-temperature one at 510–1000 °C. The reductive property of the B-site metals of Fe and Co are reflected in the TPR patterns. That is because Gd ion in the A-site does not take part in the H_2 reduction reaction. According

to the published data [12], the low-temperature reduction region is associated with the $Me^{3+} \rightarrow Me^{2+}$ transition, and the broad recovery peaks in the high-temperature region are associated with the $Me^{2+} \rightarrow Me^{0}$ transition. For compounds $GdCoO_3$ and $GdFeO_3$, the reduction temperatures of the first peaks were higher than that of the Co_2O_3 and Fe_2O_3 oxides, for which a two-stage reduction was also observed. As a result, we concluded that the reduction of Co and Fe in the perovskite structure is more complicated than in the simple oxides, which may be due to the gadolinium effect. In addition, with the increase in the iron content, the second reduction peaks shifted to a higher temperature range, and their intensity decreased. This indicated the inhibitory role of iron in cobalt reduction and the decline in the quantity of the reductive bulk lattice oxygen that can be assigned to the movement of lattice oxygen from the interior to subsurface or surface by substitution-induced oxygen defective sites [27]. For compounds $GdFe_{0.2}Co_{0.8}O_3$ (x = 0.8) and $GdFe_{0.5}Co_{0.5}O_3$ (x = 0.5), the additional small reduction peaks were observed at 350 °C, 357 °C, and 468 °C, respectively, which may be due to the presence of the impurity phases of iron oxide in the low-valence state, being consistent with the results of ICP and XPS for $GdFe_{0.2}Co_{0.8}O_3$ (x = 0.8).

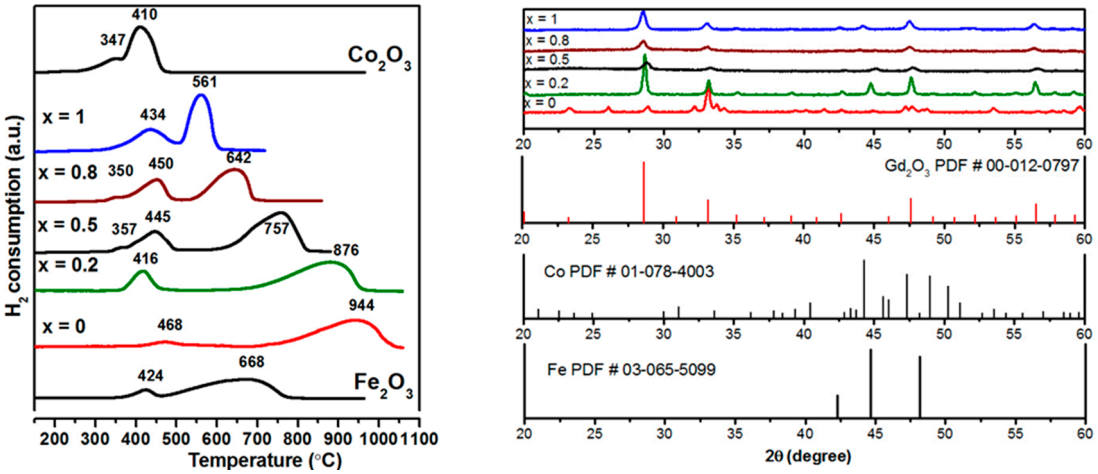

Figure 3. (**a**) H_2-TPR profiles for each sample; (**b**) XRD patterns of $GdFe_{1-x}Co_xO_3$ after reduction at 900 °C.

Table 3. H_2-TPR profiles analysis data.

Samples	Reduction Temperature (°C)		H_2 Consumed, μmol/g		
	Peak 1 ($Me^{3+} \rightarrow Me^{2+}$)	Peak 2 ($Me^{2+} \rightarrow Me^{0}$)	Peak 1	Peak 2	Total
$GdFeO_3$	468	944	141	752	893
$GdFe_{0.8}Co_{0.2}O_3$	416	876	186	806	991
$GdFe_{0.5}Co_{0.5}O_3$	445	757	296	799	1095
$GdFe_{0.2}Co_{0.8}O_3$	450	642	329	544	874
$GdCoO_3$	434	561	381	592	974

To investigate the change in the phase composition after the reduction process, all compounds were heated up to 900 °C in a H_2 flow, and Figure 3b shows the results. The diffraction patterns of all cobalt-containing compounds after reduction show the absence of the diffraction peaks characteristic for perovskites that indicates the destruction of the perovskite structure and its conversion to Gd_2O_3 (PDF-ICDD 00-012-0797), metal Co (PDF-ICDD 01-078-4003), and metal Fe (PDF-ICDD 03-065-5099). As for $GdFeO_3$ (x = 0), the diffraction pattern obtained after the processing of the sample at 900 °C in a reducing atmosphere shows the presence of reflections of the phase $GdFeO_3$ (PDF-ICDD 01-072-

9908) and a small peak related to Gd_2O_3 (PDF-ICDD 00-012-0797) associated with a high reduction temperature for this sample (peak at 944 °C, Figure 3a).

Temperature-programmed desorption of oxygen [28] is a simple and direct method to determine oxygen vacancies. Generally, for compounds of this class, two areas of oxygen desorption are observed. The first desorption peak appears at temperatures up to 700 °C and is referred to as oxygen (α-O_2) bonded to oxygen adsorbed on surface oxygen vacancies [29]. The second peak, which, as a rule, can be observed at temperatures above 750 °C, relates to β-O_2, which is usually referred to as oxygen that diffuses from the bulk and is considered an indicator of oxygen mobility in the structure [30]. Figure 4a,b show the STA and TPD-O_2 curves for the studied compounds. No obvious desorption peaks appeared up to 700 °C, possibly due to the small specific surface area. At the same time, with an increase in the cobalt content, an increase in the area of oxygen desorption was observed at temperatures above 750 °C indicating better mobility of bulk oxygen and increases in the order: $GdFeO_3 \approx GdFe_{0.8}Co_{0.2}O_3 < GdFe_{0.5}Co_{0.5}O_3 < GdFe_{0.2}Co_{0.8}O_3 < GdCoO_3$. The tendency towards an increase in the β-O_2 content with an increase in the Co content was in good agreement with the H_2-TPR data and confirmed that there are a large number of cationic vacancies in the Co-rich samples due to the easier Co^{3+} into Co^{2+} transition.

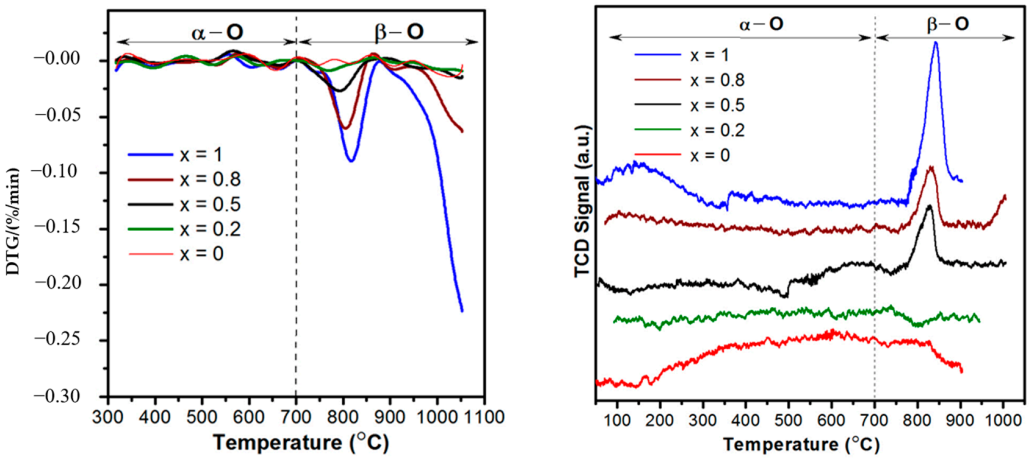

(**a**) (**b**)

Figure 4. (**a**) STA; (**b**) TPD-O_2 curves of $GdFe_{1-x}Co_xO_3$.

To exclude the influence of impurities (CO_2, etc.) STA experiment in the air (spectra are not shown) was performed. The absence of the mass loss in the range of 40–1000 °C was observed, confirming that the effects observed on the TPD-O_2 and STA curves were associated with the oxygen desorption (Figure 4a,b).

Thermogravimetric analysis (TGA) in the air atmosphere is usually used as an effective method to study the catalytic characteristics of soot burning. The soot combustion temperature obtained from the TGA data was used as an indicator of catalyst efficiency [31]. The simultaneous thermal analysis (STA-TGA) was used to study the catalytic activity of the samples in the soot oxidation process. It was carried out in a synthetic air atmosphere in the temperature range of 70–900 °C and under tight contact conditions.

Figure 5 shows the TG and DTG curves for a simulation of diesel soot oxidation for the $GdFe_{1-x}Co_xO_3$ (x = 0; 0.2; 0.5; 0.8; 1) catalysts. Non-catalytic soot oxidation occurs at 550–700 °C (DSC peak at 670 °C). The addition of perovskites leads to the low-temperature shift of soot oxidation, i.e., synthesized perovskites are catalytically active in this reaction. It can be seen that the increase of the catalytic activity in the line of samples $GdFe_{0.5}Co_{0.5}O_3 < GdFe_{0.2}Co_{0.8}O_3 < GdCoO_3$ that is in good agreement with H_2-TPR, TPD-O_2, and STA results. Thus, the increase of the activity linearly correlated with the reaction ability and amount of β-O_2 of perovskite for the Co-rich sample. It was shown that an increase in the amount of Co leads to a change in the crystal lattice parameters (XRD) and a change in

the valence states (XPS). These changes of the perovskite structure provided the increased reaction ability of β-O_2 that was shown by TPD-O_2 and STA results. This provided the increased reaction ability of the surface in the oxidative reaction of oxidation that H2-TPR showed.

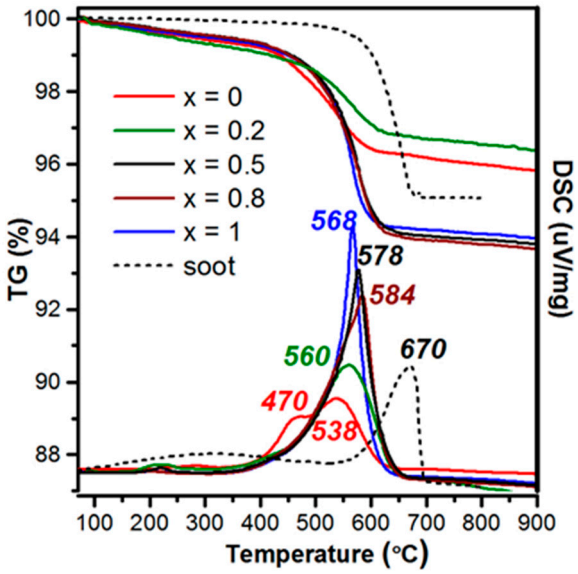

Figure 5. TGA and DSC curves for soot oxidation over $GdFe_{1-x}Co_xO_3$ (x = 0; 0.2; 0.5; 0.8; 1) catalysts.

The perovskites with high loading of Fe are characterized by the double peaks of soot combustion that indicate the different oxidation mechanisms or different active sites compared with the one over Co-rich perovskites. These phenomena may be described as the results of the inhomogeneous structure of the samples. Thus, the impurities of iron oxides were found in these samples by a complex of methods. The highest activity of $GdFeO_3$ was also associated with the highest specific surface area that played an important role because of the occurrence of reaction on the contact between the catalyst particles and soot. Thus, for the Fe-rich sample, the reaction ability of the surface was associated with both iron oxide and increased surface area of the perovskite phase.

Thus, the correlation between compositions of $GdFe_{1-x}Co_xO_3$ perovskites, their structure, reaction ability, and catalytic properties in the reaction of soot combustion was found. The substitution of Fe ions by Co ions led to an improvement in the redox properties, and the Fe/Co in $GdFe_{1-x}Co_xO_3$ (x = 0; 0.2; 0.5; 0.8; 1) provided stability and catalytic characteristics.

3. Materials and Methods

A series of $GdFe_{1-x}Co_xO_3$ (x = 0; 0.2; 0.5; 0.8; 1) perovskite-type oxides was prepared by the sol-gel method as detailed elsewhere [32]. $Gd(NO_3)_3{\cdot}5H_2O$ (99.9%, Vecton, St. Petersburg, Russia), $Co(NO_3)_2{\cdot}6H_2O$ (98%, Vecton, St. Petersburg, Russia) and $Fe(NO_3)_3{\cdot}9H_2O$ (98.5%, Vecton, St. Petersburg, Russia) were used as reagents, citric acid monohydrate (molar ratio of citric acid/metals = 2:1) was used as the complexing agent, and the aqueous solution of ammonia was used as a precipitation agent. The metal precursors and citric acid were weighed in stoichiometric proportions and dissolved in distilled water. Ammonia water was added to the aqueous solution dropwise under vigorous stirring until a pH of 7 was reached. After thermal dehydration at ~90 °C on a hot plate (to remove the excess solvent), these turned into highly viscous liquids. As soon as the viscous liquids had been formed, the hot plate temperature was increased up to ~240 °C. At this stage, viscous liquids swelled and auto-ignited with the rapid evolution of a large volume of gases to produce voluminous powders. The powders obtained after the auto-ignition were calcined at 500 °C for 2 h.

3.1. Characterization

XRD analysis data were collected with a Rigaku MiniFlex II (Rigaku, Akishima-shi, Tokyo) diffractometer (powder X-ray diffraction, CuKα radiation, 2θ = 20–60°). Elemental analysis of the samples was carried out by inductively coupled plasma (ICP) using an ICPE-9000 spectrometer (Shimadzu Europa GmbH, Duisburg, Germany) after the dissolution of the solids in acidic media (in a mixture of 5 mL of concentrated HNO_3 and 1 mL of concentrated HF). The specific surface area (S_{BET}) and a pore size distribution of the samples were determined by N_2 sorption at −196 °C using a 3Flex analyzer (Micromeritics, Norcross, GA, USA). Prior to the analysis, all samples were outgassed at 200 °C under vacuum for 2 h. The specific surface area was calculated using the Brunauer–Emmett–Teller (S_{BET}) method. Elemental compositions and valence band positions were determined from X-ray photoelectron spectra (XPS) recorded on a Escalab 250Xi spectrometer(Thermo Fisher Scientific, UK), Al Kα radiation, 1486.6 eV; spectral resolution, 0.5 eV; the reference carbon line Cls (C–C bond) was observed at binding energy (BE) of 284.8 eV.

The temperature-programmed reduction in hydrogen (H_2-TPR) was carried out in a Micrometrics AutoChem equipment (Norcross, Georgia, United States) interfaced to a data station. About 35 mg of the catalyst were pretreated under dry argon at 180 °C for 0.5 h. The TPR profile was recorded by heating the sample from room temperature (around 25 °C) to up to 1000 °C at a rate of 10 °C min^{-1} under a flowing of 10 vol.% H_2/Ar. The hydrogen consumption was monitored with a thermal conductivity detector (TCD). The effluent gas was passed through a cold trap placed before the TCD to avoid water condensation from the outlet stream.

The temperature-programmed desorption of oxygen (TPD-O_2) was studied in a Micrometrics AutoChem HP 2950 (Norcross, Georgia, United States). About 0.2 g of the sample was pretreated at 800 °C with a purge of flowing O_2 gas at a 20 mL/min rate followed by the cooling down to room temperature at a ramp of 10 °C/min. Then the sample was heated from 30 to up to 1000 °C under a flowing of pure He. A TCD monitored the signal of desorbed oxygen. The investigation of the oxides' stability was performed by thermogravimetric analysis (TG 209 F1 Libra, NETZSCH-Gerätebau GmbH, Selb, Germany), and additionally by simultaneous thermal analysis (STA, TG + DSC Netzsch STA449 F1 Jupiter, Selb, Germany) coupled with quadrupole mass spectrometer (QMS 403C Aëolos) to determine the composition of the gases released during the heating. Thermal analysis was performed using 25–30 mg samples at a heating rate of 10 °C/min in the temperature range of 30–1000 °C in a 100 mL/min oxidizing atmosphere flow. Oxygen storage capacity (OSC) was measured by TG (Netzsch TG 209 F1 Libra), and additionally by simultaneous thermal analysis (STA, TG + DSC Netzsch STA449 F1 Jupiter) coupled with quadrupole mass spectrometer (QMS 403C Aëolos). The sample (about 50 mg) was pretreated in Ar (30 mL/min) by heating from 25 to up to 950 °C (ramp rate was 10 °C/min). Then the sample was cooled down under an inert atmosphere up to 300 °C. At 300 °C, the sample was saturated with 20% O_2 in Ar (30 mL/min) and cooled down to 25 °C, still under O_2. Finally, the sample was treated under Ar (30 mL/min) heating from room temperature up to 800 °C (ramp rate was 5 °C/min).

3.2. Catalytic Testing

The simultaneous thermal analysis (STA-TGA) was used to study the samples' catalytic activity in soot combustion. The tests were carried out using the thermogravimeter STA 449F1. The TGA was performed in an air flow with a temperature range of 70–1000 °C and a heating rate of 10 °C/min. A simulated model diesel soot substance was prepared by mixing the prepared catalyst with 5 wt.% carbon black (Micromeritics, USA); the catalyst and carbon black were intensively mixed using an agate mortar for 15 min (to obtain the tight contact).

4. Conclusions

The oxides with the composition $GdFe_{1-x}Co_xO_3$ (x = 0; 0.2; 0.5; 0.8; 1) were successfully obtained by the sol-gel method. The XRD results showed an increase in the Co content showed a shift of diffraction peaks confirming the formation of solid solutions and the Co incorporation into the perovskite structures. The XPS results made it possible to determine the surface composition and refine the state of metal cations. It was found that the metals are in the heterovalent state of Co^{2+}/Co^{3+} and Fe^{2+}/Fe^{3+}, and from the O1s analysis, it was found that the O_s/O_l ratio increases in the series and correlates with the S_{BET} results. The H_2-TPR experiments demonstrated that an increase in the cobalt fraction in the studied compounds led to a decrease in the reduction temperature and improved the oxygen mobility, thereby improving the redox properties. The results of evaluating the obtained compounds' activity in the catalytic oxidation of diesel soot correlated well with all the results obtained.

This work is the first step of in studying the catalytic properties of perovskites $GdFe_{1-x}Co_xO_3$ (x = 0; 0.2; 0.5; 0.8; 1) in the oxidation reaction of diesel soot. In the future, we plan to study the catalytic parameters in more detail, expand the study of the effect of the type and degree of substitution of metals in A/B-position on the catalytic and physicochemical characteristics of perovskites $A_{1-x}A'_xB_{1-y}B'_yO_{3\pm\delta}$, as well as improve the synthesis methods for obtaining perovskites with a large surface area.

Author Contributions: Conceptualization and methodology I.A.Z. and G.V.M.; investigation, I.V.C. and L.V.Y.; writing—review and editing, L.V.Y., O.I.S. and I.A.Z. All authors have read and agreed to the published version of the manuscript.

Funding: This work was supported by the Scholarship and grant of the president of the Russian Federation (No. СП-1164.2019.1 and MK-480.2020.3). The TPx and STA studies were carried out with the support of grant RSBR No. 19-33-50079 mol_nr.

Data Availability Statement: Data sharing is not applicable to this article.

Acknowledgments: Authors are also grateful to Saint Petersburg State University Research Park. TG and DSC studies were carried out in the Center of Thermal Analysis and Calorimetry, XRD study was carried out in Research Centre for X-ray Diffraction Studies, XPS study was performed at Resource Center for Studies in Surface Science, ICP study was carried out in Center for chemical analysis and materials research.

Conflicts of Interest: The authors declare no conflict of interest.

References

1. Omidvarborna, H.; Kumar, A.; Kim, D.S. Recent studies on soot modeling for diesel combustion. *Renew. Sustain. Energy Rev.* **2015**, *48*, 635–647. [CrossRef]
2. Uppara, H.P.; Pasuparthy, J.S.; Pradhan, S.; Singh, S.K.; Labhsetwar, N.K.; Dasari, H. The comparative experimental investigations of $SrMn(Co^{3+}/Co^{2+})O_{3\pm\delta}$ and $SrMn(Cu^{2+})O_{3\pm\delta}$ perovskites towards soot oxidation activity. *Mol. Catal.* **2019**, *482*, 110665. [CrossRef]
3. Castillo Marcano, S.J.; Bensaid, S.; Deorsola, F.A.; Russo, N.; Fino, D. Multifunctional catalyst based on $BaO/Pt/CeO_2$ for NO_2-assisted soot abatement and NO_x storage. *Fuel* **2015**, *149*, 78–84. [CrossRef]
4. Yamazaki, K.; Kayama, T.; Dong, F.; Shinjoh, H. A mechanistic study on soot oxidation over CeO_2-Ag catalyst with 'rice-ball' morphology. *J. Catal.* **2011**, *282*, 289–298. [CrossRef]
5. Guo, X.; Meng, M.; Dai, F.; Li, Q.; Zhang, Z.; Jiang, Z.; Zhang, S.; Huang, Y. NO_x-assisted soot combustion over dually substituted perovskite catalysts $La_{1-x}K_xCo_{1-y}Pd_yO_{3-\delta}$. *Appl. Catal. B Environ.* **2013**, *142–143*, 278–289. [CrossRef]
6. Yi, Y.; Liu, H.; Chu, B.; Qin, Z.; Dong, L.; He, H.; Tang, C.; Fan, M.; Bin, L. Catalytic removal NO by CO over $LaNi_{0.5}M_{0.5}O_3$ (M = Co, Mn, Cu) perovskite oxide catalysts: Tune surface chemical composition to improve N_2 selectivity. *Chem. Eng. J.* **2019**, *369*, 511–521. [CrossRef]
7. Farhang, Y.; Taheri-Nassaj, E.; Rezaei, M. Pd doped $LaSrCuO_4$ perovskite nano-catalysts synthesized by a novel solid state method for CO oxidation and Methane combustion. *Ceram. Int.* **2018**, *44*, 21499–21506. [CrossRef]
8. Kucharczyk, B.; Okal, J.; Tylus, W.; Winiarski, J.; Szczygieł, B. The effect of the calcination temperature of $LaFeO_3$ precursors on the properties and catalytic activity of perovskite in methane oxidation. *Ceram. Int.* **2019**, *45*, 2779–2788. [CrossRef]
9. Sihaib, Z.; Puleo, F.; Pantaleo, G.; La Parola, V.; Valverde, J.L.; Gil, S.; Liotta, L.F.; Giroir-Fendler, A. The effect of citric acid concentration on the properties of $LaMnO_3$ as a catalyst for hydrocarbon oxidation. *Catalysts* **2019**, *9*, 226. [CrossRef]

10. Fang, S.; Wang, L.; Sun, Z.; Feng, N.; Shen, C.; Lin, P.; Wan, H.; Guan, G. Catalytic removal of diesel soot particulates over K and Mg substituted $La_{1-X}K_xCo_{1-y}Mg_yO_3$ perovskite oxides. *Catal. Commun.* **2014**, *49*, 15–19. [CrossRef]
11. Forni, L.; Rossetti, I. Catalytic combustion of hydrocarbons over perovskites. *Appl. Catal. B Environ.* **2002**, *38*, 29–37. [CrossRef]
12. Merino, N.A.; Barbero, B.P.; Eloy, P.; Cadús, L.E. $La_{1-x}Ca_xCoO_3$ perovskite-type oxides: Identification of the surface oxygen species by XPS. *Appl. Surf. Sci.* **2006**, *253*, 1489–1493. [CrossRef]
13. Lim, H.S.; Lee, M.; Kang, D.; Lee, J.W. Role of transition metal in perovskites for enhancing selectivity of methane to syngas. *Int. J. Hydrogen Energy* **2018**, *43*, 20580–20590. [CrossRef]
14. Dai, X.P.; Wu, Q.; Li, R.J.; Yu, C.C.; Hao, Z.P. Hydrogen production from a combination of the water-gas shift and redox cycle process of methane partial oxidation via lattice oxygen-over $LaFeO_3$ perovskite catalyst. *J. Phys. Chem. B.* **2006**, *110*, 25856–25862. [CrossRef]
15. Dai, X.; Yu, C.; Li, R.; Wu, Q.; Shi, K.; Hao, Z. Effect of calcination temperature and reaction conditions on methane partial oxidation using lanthanum-based perovskite as oxygen donor. *J. Rare Earths* **2008**, *26*, 341–346. [CrossRef]
16. Yafarova, L.; Silyukov, O.; Kryuchkova, T.; Sheshko, T.; Zvereva, I. The influence of Fe substitution in $GdFeO_3$ on redox and catalytic properties. *Russ. J. Phys. Chem. A* **2020**, *13*, 2679–2684. [CrossRef]
17. Kryuchkova, T.; Kost', V.; Sheshko, T.; Chislova, I.; Yafarova, L.; Zvereva, I. Effect of Cobalt in $GdFeO_3$ Catalyst Systems on Their Activity in the Dry Reforming of Methane to Synthesis Gas. *Pet. Chem.* **2020**, *5*, 57–64. [CrossRef]
18. Sheshko, T.F.; Sharaeva, A.A.; Powella, O.K.; Serov, Y.M.; Chislova, I.V.; Yafarova, L.V.; Koroleva, A.V.; Zvereva, I.A. Carbon Oxide Hydrogenation over GdBO3 (B = Fe, Mn, Co) Complex Oxides: Effect of Carbon Dioxide on Product Composition. *Pet. Chem.* **2020**, *5*, 17–23. [CrossRef]
19. Dyck, C.R.; Peterson, R.C.; Yu, Z.B.; Krstic, V.D. Crystal structure, thermal expansion and electrical conductivity of dual-phase $Gd_{0.8}Sr_{0.2}Co_{1-y}Fe_yO_{3-\delta}$ ($0 \leq y \leq 1.0$). *Solid State Ion.* **2005**, *176*, 103–108. [CrossRef]
20. Marezio, M.; Remeika, J.; Dernier, P. The crystal chemistry of the rare earth orthoferrites. *Acta Crystallogr. Sect. B Struct. Crystallogr. Cryst. Chem.* **1970**, *26*, 2008–2022. [CrossRef]
21. Nedil'ko, S.A.; Ermakova, M.N.; Lyashko, M.N.; Gozhdzinskii, S.M. Rare Earth Metal Cobaltates (III). 1979.
22. Zhao, K.; Shen, Y.; Huang, Z.; He, F.; Wei, G.; Zheng, A.; Li, H.; Zhao, Z. Different oxidation routes for lattice oxygen recovery of double-perovskite type oxides $LaSrFeCoO_6$ as oxygen carriers for chemical looping steam methane reforming. *J. Energy Chem.* **2017**, *26*, 501–509. [CrossRef]
23. Graat, P.C.J.; Somers, M.A.J. Simultaneous determination of composition and thickness of thin iron-oxide films from XPS Fe 2p spectra. *Appl. Surf. Sci.* **1996**, *100–101*, 36–40. [CrossRef]
24. Tholkappiyan, R.; Vishista, K. Tuning the composition and magnetostructure of dysprosium iron garnets by Co-substitution: An XRD, FT-IR, XPS and VSM study. *Appl. Surf. Sci.* **2015**, *351*, 1016–1024. [CrossRef]
25. Wang, Y.; Ren, J.; Wang, Y.; Zhang, F.; Liu, X.; Guo, Y.; Lu, G. Nanocasted synthesis of mesoporous $LaCoO_3$ perovskite with extremely high surface area and excellent activity in methane combustion. *J. Phys. Chem. C.* **2008**, *112*, 15293–15298. [CrossRef]
26. Bhattacharya, A.; Chu, X.; Gao, Q.; Li, X.; Dong, Y.; Liang, S.; Chakraborty, A.K. Influence of Gd^{+3} Incorporation on Ethanol Sensing Properties of Barium Stannate Microrod Films Prepared by Coprecipitation Method. *Appl. Surf. Sci.* **2019**, *504*, 144289. [CrossRef]
27. Wu, Y.; Li, L.; Chu, B.; Yi, Y.; Qin, Z.; Fan, M.; Qin, Q.; He, H.; Zhang, L.; Dong, L.; et al. Catalytic reduction of NO by CO over B-site partially substituted $LaM_{0.25}Co_{0.75}O_3$ (M = Cu, Mn, Fe) perovskite oxide catalysts: The correlation between physicochemical properties and catalytic performance. *Appl. Catal. A Gen.* **2018**, *568*, 43–53. [CrossRef]
28. Barbero, B.P.; Gamboa, J.A.; Cadús, L.E. Synthesis and characterisation of $La_{1-x}Ca_xFeO_3$ perovskite-type oxide catalysts for total oxidation of volatile organic compounds. *Appl. Catal. B Environ.* **2006**, *65*, 21–30. [CrossRef]
29. Levasseur, B.; Kaliaguine, S. Effect of the rare earth in the perovskite-type mixed oxides $AMnO_3$ (A = Y, La, Pr, Sm, Dy) as catalysts in methanol oxidation. *J. Solid State Chem.* **2008**, *181*, 2953–2963. [CrossRef]
30. Kaliaguine, S.; Van Neste, A.; Szabo, V.; Gallot, J.E.; Bassir, M.; Muzychuk, R. Perovskite-type oxides synthesized by reactive grinding. Part I. Preparation and characterization. *Appl. Catal. A Gen.* **2001**, *209*, 345–358. [CrossRef]
31. Bueno-López, A.; Krishna, K.; Makkee, M.; Moulijn, J.A. Enhanced soot oxidation by lattice oxygen via La^{3+}-doped CeO_2. *J. Catal.* **2005**, *230*, 237–248. [CrossRef]
32. Yafarova, L.V.; Chislova, I.V.; Zvereva, I.A.; Kryuchkova, T.A.; Kost, V.V.; Sheshko, T.F. Sol–gel synthesis and investigation of catalysts on the basis of perovskite-type oxides $GdMO_3$ (M = Fe, Co). *J. Sol-Gel Sci. Technol.* **2019**, *92*, 264–272. [CrossRef]